Structure of Gel Phase DMPC Determined by X-Ray Diffraction

Stephanie Tristram-Nagle,* Yufeng Liu,† Justin Legleiter,‡ and John F. Nagle*†
*Department of Biological Sciences, †Department of Physics, ‡Department of Chemistry, Carnegie Mellon University, Pittsburgh, Pennsylvania 15213 USA

ABSTRACT The structure of fully hydrated gel phase dimyristoylphosphatidylcholine lipid bilayers was obtained at 10°C. Oriented lipid multilayers were used to obtain high signal-to-noise intensity data. The chain tilt angle and an estimate of the methylene electron density were obtained from wide angle reflections. The chain tilt angle is measured to be 32.3 ± 0.6° near full hydration, and it does not change as the sample is mildly dehydrated from a repeat spacing of $D = 59.9$ Å to $D = 56.5$ Å. Low angle diffraction peaks were obtained up to the tenth order for 17 samples with variable D and prepared by three different methods with different geometries. In addition to the usual Fourier reconstructions of the electron density profiles, model electron density profiles were fit to all the low angle data simultaneously while constraining the model to include the wide-angle data and the measured lipid volume. Results are obtained for area/lipid ($A = 47.2 \pm 0.5$ Å^2), the compressibility modulus ($K_A = 500 \pm 100$ dyn/cm), various thicknesses, such as the hydrocarbon thickness ($2D_C = 30.3 \pm 0.2$ Å), and the head-to-head spacing ($D_{HH} = 40.1 \pm 0.1$ Å).

INTRODUCTION

Because lipid bilayers form the underlying matrix of cell membranes, it is desirable to measure their structural parameters quantitatively. The hydrocarbon thickness of the bilayer is important for accommodation of transmembrane proteins (Lewis and Engelman, 1983; Veld et al., 1991; Lundbaek and Andersen, 1999) and for permeability of small molecules (Paula et al., 1996; Huster et al., 1997; Olbrich et al., 2000). Obtaining the water spacing between adjacent bilayers is required for evaluating interactions between membranes (Rand and Parsegian, 1989; McIntosh, 2000; Nagle and Tristram-Nagle, 2000). The area/molecule provides a test and guide for simulations of lipid bilayers (Tobias et al., 1997; Tieleman et al., 1997; Feller et al., 1997; Venable et al., 2000).

Although most cell membranes in vivo exist in the fluid L_α phase, the gel phase of lipid bilayers has biological interest for specialized membranes such as stratum corneum (Bouwstra et al., 1992; Pilgram et al., 1999). In addition, gel phase structure has broader relevance because one method for obtaining fluid $L\alpha$ phase structure uses gel phase structure as an essential stepping stone (McIntosh and Simon, 1986a; Nagle et al., 1996). This method can be used for any fluid phase lipid with the same headgroup, even if the fluid phase of the lipid in question does not have a gel phase (Tristram-Nagle et al., 1998; Petrache et al., 1998a; Nagle and Tristram-Nagle, 2000). Therefore, the best determination of any gel phase bilayer structure of a phosphatidylcholine lipid is of general interest.

DPPC (dipalmitoylphosphatidylcholine) is the most studied gel phase structure. The pioneering work of Torbet and Wilkins (1976) obtained 10 orders of diffraction for fully hydrated multilamellar vesicles (i.e., MLV powder sample) as well as for less fully hydrated oriented samples. Their electron density profiles and their continuous Fourier transforms of the electron density were different for their oriented samples than for their fully hydrated powder sample. Their fully hydrated sample had a lamellar repeat spacing $D = 64.0$ Å, but all their oriented samples had D less than 58.8 Å with no data within the gap from $D = 64.0$ Å to $D = 58.8$ Å. Repeated observation of such gaps over the years led to the concept of the vapor pressure paradox (Rand and Parsegian, 1989). However, full hydration of the oriented gel phase of DPPC from water vapor was accomplished some time ago (Katsaras et al., 1992; Tristram-Nagle et al., 1993), and this has now been accomplished for the fluid phase (Katsaras, 1998; Nagle and Katsaras, 1999; Lyatskaya et al., 2001). As the results in this article show for gel phase dimyristoylphosphatidylcholine (DMPC), the considerable osmotic pressure associated with a 5 Å difference in D causes a decrease in chain tilt, thereby increasing the hydrocarbon thickness. This changes the electron density profile and the continuous transform, in agreement with the results of Torbet and Wilkins (1976) for DPPC. However, milder dehydration associated with less osmotic pressure reduces the chain tilt imperceptibly, as we show in this paper. Therefore, it is now possible to obtain data in a range of D spacings from fully hydrated to 4 Å less than fully hydrated in which the structure does not change measurably and to obtain 10 orders of diffraction from oriented samples. The closest comparison is the study of McIntosh and Simon (1986b), which obtained five orders of diffraction for unoriented samples of gel phase DPPC with D spacings from 63.6 to 57.8 Å with the conclusion that changes in bilayer thickness were less than 1 Å. Having a range of D spacings provides many more data points that give a more accurate continuous Fourier transform. In this paper, we take advantage of this increase in the amount and quality of data by

Submitted March 19, 2002, and accepted for publication July 15, 2002.
Address reprint requests to John F. Nagle, Department of Physics, 5000 Forbes Avenue, Carnegie Mellon University, Pittsburgh, PA 15213. Tel.: 412-268-2764; Fax: 412-681-0648; E-mail: nagle@andrew.cmu.edu.

0006-3495/02/12/3324/12 $2.00

developing a global analysis that uses all the data simultaneously to determine the gel phase structure of DMPC.

MATERIALS AND METHODS

DMPC (1,2-dimyristoyl-*sn*-glycero-phosphatidylcholine) was purchased from Avanti Polar Lipids (Alabaster, AL) in the lyophilized form and used without further purification. Organic solvents were high-performance liquid chromatography grade from Aldrich (Milwaukee, WI).

Oriented sample preparation

Oriented samples were prepared using the "rock and roll" method (Tristram-Nagle et al., 1993) in which 5 or 10 mg of lipid is deposited onto a flat substrate (3 × 4 cm piece of freshly cleaved mica or glass microscope slide) by evaporating from a chloroform:methanol mixture (2.5:1, v/v), or from a trifluoroethanol:chloroform mixture (2:1, v/v). This method obtained greater than 80% orientation according to a magic angle spinning NMR assay (K. Gawrisch, private communication). After drying for 1 day in a glove box followed by 1 day on the laboratory bench and transferring to x-ray sample chambers, full hydration through the vapor was hastened using a Peltier element to cool the lipid film relative to the water vapor, thereby condensing water onto the lipid (Tristram-Nagle et al., 1993). Mild dehydration in watertight chambers with high relative humidity was effected by reversing the electrical leads to the Peltier cooler to maintain the sample slightly warmer than the water vapor in the chamber. The thickness of the sample (required for the x-ray absorption correction) was estimated by two different methods: 1) calculation using the lipid mass and substrate area covered and 2) atomic force microscopy (AFM).

AFM

Tapping mode AFM in air and under water was performed with a Nanoscope III-M system (Digital Instruments, Santa Barbara, CA), equipped with a vertical-engage J scanner. Standard etched silicon probes (spring constant 50 N/m, resonance frequency 300 kHz) were used for studies of dried samples conducted in air. Typical imaging parameters were: cantilever oscillation 0.2 to 0.7 V with set points 250 to 500 kHz, scan frequencies 0.99 to 2.99 Hz, image resolution 512 by 512 points. Dried samples sometimes contained holes of 0.1- to 10-μm diameter. The film thickness was measured from either the bottom of the larger holes or from substrate that had been cleaned by a knife-edge to the top of the adjacent lipid film. For samples that had a nominal calculated thickness of 10 μm, AFM results for average thickness were 6.7 μm with average variations in the thickness of 2.4 μm, which were far larger than intrinsic errors in the AFM method. For samples with calculated thickness of 5 μm, the AFM average was approximately 3 μm. The AFM result was used as the true thickness of dried lipid because some lipid builds up near the edges of the mica sheet during the rock and roll procedure, and this lipid does not contribute to the diffraction. For samples not observed by AFM, a factor of two-thirds was applied to the calculated thickness. Under water, tapping mode AFM in a fluid cell was made possible by applying a sinusoidal voltage across the *z* direction of the piezoelectric scanner after minor modification of the instrument. A wide-legged silicon nitride cantilever (spring constant, 0.58 N/m) was used with oscillation amplitude centered on 8 to 9 kHz, instead of 300 kHz as in the dry condition. Holes were less evident when the sample was immersed in water (Fig. 1), suggesting that hydration may have promoted annealing of irregularities in the sample.

Diffraction from cylindrical samples

The thin (~30 μm) flexible mica substrate with a film of DMPC was fixed tightly to a curved glass beaker (radius = 17.5 mm) with epoxy. The cylinder was mounted horizontally into a specially constructed x-ray chamber (Katsaras and Watson, 2000). Both low- and wide-angle data were obtained at the D-1 station at the Cornell High Energy Synchrotron Source (CHESS). X-rays were selected with $\lambda = 1.4033$ Å for part of the data and $\lambda = 1.2727$ Å on another run, using the CHESS monochromator consisting of two W/B_4C (2:1) multilayers (Osmic, Detroit, MI) with 1.5% (full width half maximum) (FWHM) energy dispersion. By detuning the angle between the two multilayers slightly, the fraction of $\lambda/2$ radiation was reduced from 0.012 to 0.002. Angular q_r resolution of 0.001 Å^{-1} was achieved using slits, and q_z resolution was limited by the energy dispersion of the monochromator. X-ray exposure times varied from less than 1 s so as not to overexpose the $h = 1$ order, to 1 to 2 min to obtain good signal/noise for the highest orders. A sequence of 30 1-min scans was taken at the same spot to judge x-ray damage by monitoring the change in *D* spacing. Only after 15 min had the *D* spacing increased by 0.1 Å followed by an increase of 0.5 Å after 20 min. We note that for a 120 s exposure, with beam intensity of 6×10^{10} photons/second at the sample, the ratio of absorbed x-rays to the number of exposed lipid molecules was on the order of 10^{-4}, indicating minimal direct x-ray damage to the sample, and the short exposure times limit the amount of subsequent damage due to free radicals. Thin layer chromatography performed a week after the experiments also indicated less than 0.1% lysolecithin for our typical exposures that lasted less than 5 min.

Diffraction data were collected using a charge-coupled device (CCD) detector with a 2048 × 2048 pixel array with pixel size of 40.95 μm (Tate et al., 1995) and with distance to the sample of 16.57 or 21.06 cm determined using an oriented standard of silver behenate ($D = 58.367$ Å) (Blanton et al., 1995). The CCD data were corrected for geometric distortion, and variations in pixel intensity following the protocol of Barna et al. (1999) and files supplied by CHESS. Temperature was controlled with a NESLAB (Portsmouth, NH) controller and was measured with a National Institute of Science and Technology-calibrated surface probe (Yellow Springs Instruments, OH).

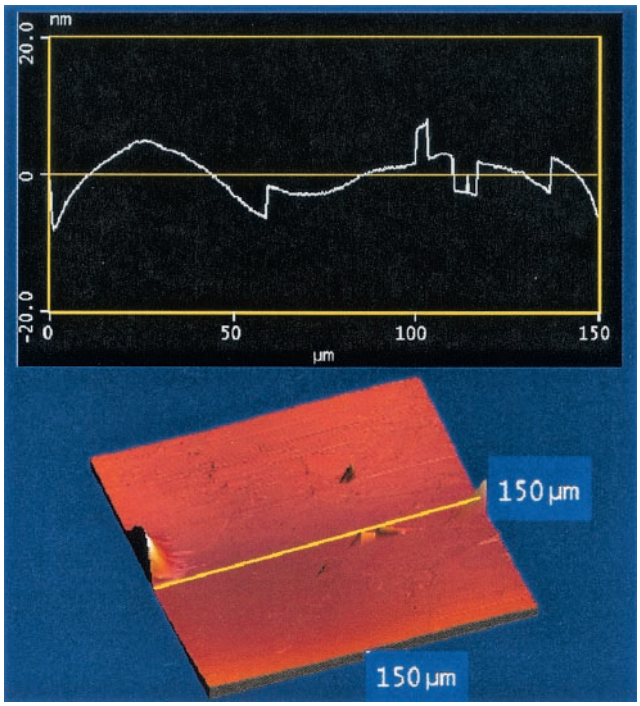

FIGURE 1 Atomic force micrograph (*bottom*) of a DMPC film of average thickness 6.7 μm on mica under water. The difference in vertical elevation between white and black colors is 0.2 μm. The elevation along the yellow line is shown in the profile at the top.

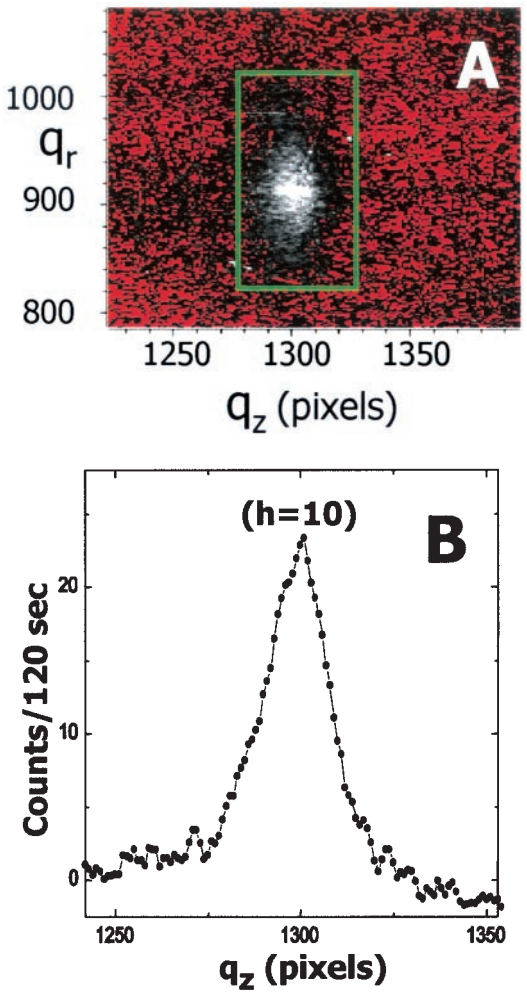

FIGURE 2 DMPC peak (h = 10) oriented on a cylindrical substrate (D = 58.2 Å). (*A*) CCD image as a function of pixel numbers in the q_z and q_r directions after background subtraction; red pixels have small (mostly 0 to −3) negative values, the gray pixels are on a gray scale from 0 to 30, and the intensity of the white pixels exceeds 30. The intensity of the peak was obtained by summing the values of all the pixels contained in the green rectangle, and the uncertainty was estimated to be 10% of the total intensity. (*b*) Intensity averaged over 140 pixels in the vertical q_r direction in *A* as a function of pixel number in the q_z direction. Instrumental q_z resolution is 15 pixels (FWHM).

For the lamellar diffraction peak intensities, background from air scattering was subtracted by interpolation from pixels outside the diffraction peaks; this background agreed well with that obtained from "light backgrounds" taken when the lipid was removed from the substrate. The diffraction peaks for these data had excellent signal/noise up to and including the tenth order, as shown in Fig. 2. Occasional higher orders could be observed but were not accurately measurable. One defect in these data occurs when the strong mica substrate peak (M1) occurring at q_z = 0.63 Å^{-1} obscures the h = 6 order (for example, see Fig. 4); however, the h = 6 order is typically quite weak, as determined using other sample preparations, so little information is lost. A weaker peak occurs from the M1 mica peak and the weak λ/2 intensity (M1/2 peak) in the vicinity of the h = 3 order and another (M3/2) occurs near the h = 9 order; intensities from these nonlipid peaks could usually be subtracted from the lipid peak intensities.

Cylindrical samples are convenient because the Bragg condition is satisfied for all orders of diffraction simultaneously, so only one CCD image must be recorded. However, for our cylinder size the location of lipid that diffracts into the h + 1 order is ~200 μm from the lipid that diffracts into the hth order, so artifacts in intensity ratio arise from variations in sample thickness around the cylinder. This artifact was shown by taking data after rotating repeatedly about the cylinder axis by the first order Bragg angle. Mapping the intensity from the different orders as a function of rotation angle yielded a thickness variation map. The worst case studied carefully was one of the less hydrated samples with D = 55.6 Å for which the nominal film thickness of 10 μm varied by a factor of two; this variation is consistent with the ±50% variation in thickness obtained by AFM.

Diffraction from flat samples

Low angle data were also obtained from flat samples of DMPC prepared by the rock and roll method on glass microscope slides that were mounted vertically in a small aluminum chamber. The main x-ray source for these samples (and also for capillary samples; see below) was a Rigaku fixed tube Cu source operated at 2.3 kW with a graphite monochromator to eliminate K_β radiation, yielding λ = 1.5418 Å. Three sets of Huber slits produced an in-plane resolution of 0.02 Å^{-1}. Temperature stability was controlled by a Lake Shore Cryotronics Model DRC-91C temperature controller (Westerville, OH), which responded to a 1000-Ω platinum resistance thermometer (Rosemount, Minneapolis, MN) in the center of the sample chamber. Data, shown in Fig. 3a, were collected using $\theta - 2\theta$ scans with a Bicron NaI scintillation counter (Solon, OH). Background was obtained from the glass slide with the lipid removed. Signal/noise was not as good for the higher orders as for the cylindrical samples measured at CHESS, and uncertainties in determining background led us to assign higher errors to the intensities of these peaks. Furthermore, $\theta - 2\theta$ scans systematically collect a smaller fraction of the total scattering for higher order peaks that are broadened by mosaic spread or fluctuations; comparison of these data with the data from cylindrical samples indicated a small systematic difference in this direction. On the other hand, for the lower orders, the entire sample was in the beam so thickness variations created less artifactual variation in relative intensities than for cylindrical samples. Footprint corrections were made for the higher orders when the entire sample was not in the beam.

Capillary samples

A fully hydrated capillary sample in excess water and a sample with a concentration of 54% polyvinylpyrrolidone (P_{osm} = 45 ± 5 atm) in the aqueous phase were prepared as described by Tristram-Nagle et al. (1998). The x-ray source was the Rigaku fixed tube, and temperature control was as for the flat samples. To observe the higher orders in these samples requires, even for rather modest signal-to-noise ratio, very long measuring times, during which the sample may be damaged by diffusing free radicals generated by x-rays (Stark, 1991). Fig. 3 *b* shows the x-ray diffraction data obtained from a fully hydrated capillary sample in excess water, in contrast with data in Fig. 3 *a* obtained from DMPC oriented onto a flat glass microscope slide. The background for the capillary sample was obtained from a glass capillary filled with water. The instrumental resolution for the capillary sample was purposely set less accurately by a factor of two compared with that for the oriented samples in an effort to increase the lipid signal, and a much longer counting time was used to try to observe the higher orders, but no orders above h = 7 were observed. The slit configuration produced slit smear (Sun et al., 1994), even in the second order peak, so the D spacings were based on orders three to five. Despite these disadvantages, capillary samples have the advantage, compared with oriented samples, that there are few geometric or sample preparation artifacts. The first four orders were measurable with high accuracy, and they were

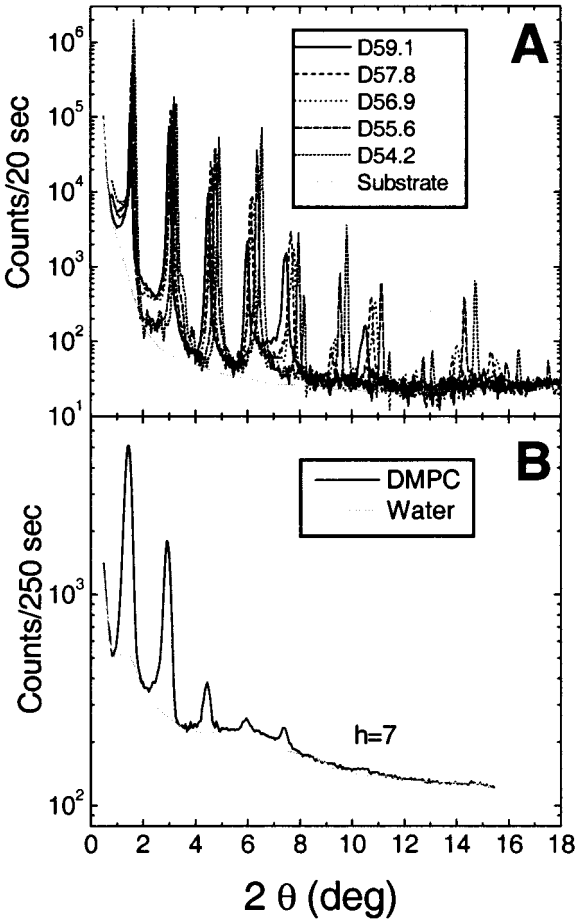

FIGURE 3 Low angle lamellar x-ray intensity data of DMPC at 10 °C. (*A*) Oriented DMPC (3 μm) on a flat glass slide with *D* spacings as shown and from a glass slide with lipid removed (*gray*); exposure times 20 s/0.05° step. (*B*) Unoriented DMPC in a capillary with $D = 59.9$ Å (*solid curve*) and a water background (*gray*); exposure times were 250 s/0.05° step for $2\theta < 8°$ and 1800 s/0.05° step for $2\theta > 8°$ (counts scaled to 250 s/0.05° step).

used with small errors in data fitting to help determine and confirm the relative intensities of orders one to four from oriented samples.

Absorption, lorentz, refraction, and reflectivity corrections

The absorption correction for flat samples of thickness *t*, absorption attenuation length μ, and for incidence angle θ is

$$\mathrm{Abs}(\theta) = [1 - \exp(-y)]/y \qquad (1)$$

in which $y = 2t/\mu\sin\theta$. For cylindrical samples, the correction formula of Wiener and White (1991) was used. Our measured $\mu = 1.0$ mm for $\lambda = 1.54$ Å agrees well with the value calculated (using http://www-cxro.lbl.gov) for the other wavelengths used at CHESS; the calculation gives $\mu = 1.5$ mm for $\lambda = 1.40$ Å and $\mu = 2.2$ mm for $\lambda = 1.27$ Å.

The usual Lorentz correction factor of *q* was applied to intensities from oriented samples, and a factor of q^2 was applied to capillary samples. Finally, the absolute values of the form factors $F_m(q_h)$ are given by

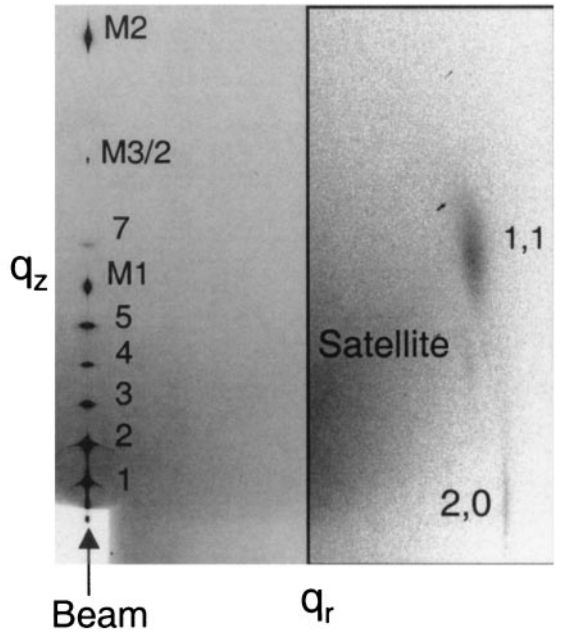

FIGURE 4 CCD image (5-s exposure) obtained from a fully hydrated cylindrical sample ($D = 59.9$Å) with q_z increasing in the vertical direction and q_r increasing in the horizontal direction. The beam and some small angle reflectivity are at the lower left, and the image of the semitransparent beamstop is the light gray area. Low angle lamellar diffraction peaks are labeled by order numbers $h = 1$ to 7. Orders 8 through 10 are not visible using the coarse gray scale necessary to visualize the lower orders. The first two orders of mica reflection are denoted M1 and M2 and the weaker M3/2 peak comes from the third order mica peak and $\lambda/2$ x-rays. The wide angle peak (20) and the peak (11) with one of its satellites (Sun et al., 1994) are shown on the right with a finer gray scale to visualize these weaker peaks.

$(K_m I_m(q_h))^{1/2}$ where the unknown scaling factor K_m for each sample *m* takes into account the relative x-ray intensities and the amount of sample.

Calculation (using http://www-cxro.lbl.gov) of the refraction of x-rays entering the lipid film from air obtains a shift in diffraction angle equivalent to an apparent decrease in *D* by 1 Å for $h = 1$. The correction is only ~0.1 Å for $h = 3$ and becomes negligible for higher orders that were primarily used to obtain *D*. No intensity correction for reflectivity from the lipid/air interface was used because less than 10^{-4} of the x-rays were reflected even near the first Bragg order.

Wide angle data

The wide angle spacings d_{11} and d_{20} were obtained by measuring from the wide angle peaks to the beam position that was well determined on the CCD image by using a semitransparent beam stop. Intensity plots located the center of the off-equator (11) peak. Although only the upper part of the (20) Bragg rod could be observed in the typical gel phase, it was quite narrow (Fig. 4) and easily extrapolated to $q_z = 0$ to yield an accurate value of d_{20}. Electron density ρ_2 of the methylene region of the bilayer was calculated using

$$\rho_2(1.27\ \text{Å}/8e) = 1/A_c = [1 - (d_{11}/2d_{20})^2]^{1/2}/(d_{20}d_{11}) \qquad (2)$$

in which 8*e* is the number of electrons per methylene and 1.27 Å is the length/methylene group along an all-*trans* hydrocarbon chain. The area perpendicular to a chain A_c is given by the standard formula for orthorhombic packing (Ruocco and Shipley, 1982; Tristram-Nagle et al., 1993).

The chain tilt angle was also obtained using standard procedures (Levine, 1973; Smith et al., 1988; Hentschel and Rusticelli, 1991; Tristram-Nagle et al., 1993). One modification arises from noting that for cylindrical samples the wide-angle scattering comes from bilayers that are oriented over a range of angles ω between the bilayer normal and the beam. Because scattering from the sample was cut off by the cylinder when $0 < \omega < \omega_{max} = 2\theta_z$, we used average values of $\sin(\omega)$ and $\cos(\omega)$ in Eq. 5 in Tristram-Nagle et al. (1993). This increases the tilt angle by less than 0.3° compared with using $\omega = 0$.

Global data analysis

Input data for the program include the corrected low angle lamellar relative intensities $I_m(q_h)$ located at q_h for m different samples. The data were fit to the 2G electron density model (Nagle and Wiener, 1989) that consists of the sum of 1) two positive Gaussians ($i = 1, 2$) to represent each of two headgroups (each Gaussian has three parameters, one for width σ_{Hi}, one for integrated size S_{Hi}, and one for location z_{Hi}), 2) a single negative Gaussian located at $z = 0$ for the four terminal methyl groups (two methyls for each lipid in each monolayer) on the hydrocarbon chains (with two parameters, one for the width σ_M and one for the integrated size defined as $2S_M$), and 3) a function that extends from $-D/2$ to $+D/2$ that has two plateaus, one for the known electron density of water ρ_w and one for the electron density of the methylene region with parameter ρ_2; the plateau function has a smooth cosine bridge with center constrained to lie between the two headgroup Gaussians and with width constrained to the average width of the headgroup Gaussians.

Given values of the model parameters, it is routine to compute the continuous transform $F(q)$ (Wiener et al., 1989). The nonlinear least squares fitting program uses simplex minimization to search for the best values of the model parameters and the unknown scale factors K_m for the relative x-ray intensities between different samples by minimizing

$$\chi^2 = \sum_{h,m} (|F_m(q_h)|^2 - I_m(q_h)K_m)^2/\sigma_{hm}^2 + W, \qquad (3)$$

in which $I_m(q_h)$ are the corrected intensity data, σ_{hm} are the estimated experimental errors for each datum $I_m(q_h)K_m$, and W is an additional term, described at the end of this subsection, that allows the model to account for other data in addition to the low angle intensities. Indeed, if there are no other data and $W = 0$, then there is a trivial solution that gives $\chi^2 = 0$ by setting $K_m = 0 = F(q)$.

Another important input datum is the volume $V_L = 1041$ Å^3 of the DMPC molecule at 10°C (Nagle and Wilkinson, 1978), which determines the product of the area/molecule A and the zero order form factor $F(0)$ through the relation (Nagle and Wiener, 1989)

$$AF(0) = 2(n_L - \rho_w V_L), \qquad (4)$$

in which $n_L = 374$ is the number of electrons/DMPC and $\rho_W = 0.3342e/$Å^3 is the electron density of water at 10°C. Because the continuous transform is (Worthington et al., 1973)

$$F(q) = \int_{-D/2}^{D/2} (\rho(z) - \rho_w)\cos(2\pi qz)dz, \qquad (5)$$

$F(0)$ depends on all the parameters in the electron density model. The area A is directly related to the wide angle data for the tilt angle θ_t, and the methylene electron density ρ_2 by

$$A = 16e/[\rho_2(1.27\text{Å})\cos\theta_t], \qquad (6)$$

in which $16e$ is the number of electrons in two methylenes, one on each of the two chains/lipid. The ratio r of terminal methyl volume V_3 to methylene volume V_2 in the hydrocarbon chains is related (Nagle and Wiener, 1989) to the parameter for the integrated size $2S_M$ of the terminal methyl Gaussian, which represents a major feature in the electron density profile, by

$$r = (9e + AS_M/2)/8e, \qquad (7)$$

in which $9e$ and $8e$ are the number of electrons per CH_3 and CH_2, respectively. The volume of the hydrocarbon chains is

$$V_C = 16e(n_2 + r)/\rho_2, \qquad (8)$$

in which n_2 is the number of methylenes/chain. The half-thickness of the hydrocarbon region is

$$D_C = V_C/A = (n_2 + r)(1.27\text{ Å})\cos\theta_t. \qquad (9)$$

The volume of the headgroup is

$$V_H = V_L - V_C. \qquad (10)$$

Finally, the ratio S_{H2}/S_{H1} of the integrated sizes of the outer to the inner headgroup Gaussian will be defined as R.

The W function in Eq. 3 includes a sum over i penalty terms, each of which has the form $(w_i - w_{i,set})^2/\sigma_i^2$. The purpose of a penalty term for a particular quantity w_i is to force the model to take into account prior information, such as from wide angle data; smaller choices for σ_i force the fitted model value of w_i closer to the value $w_{i,set}$. Any combination of penalty terms from the set [ρ_2, θ_t, r, V_H, A, D_C, R] may be chosen, although some subset combinations should not be chosen, such as [A, ρ_2, θ_t] because A is already determined from ρ_2 and θ_t by Eq. 6.

Relative electron density profiles were also routinely obtained by simple Fourier reconstruction

$$\rho(z) = \rho_W + D^{-1}F(0) + 2D^{-1}\sum_{h=1}^{hmax} F_h\cos\left(\frac{2\pi hz}{D}\right). \qquad (11)$$

RESULTS

Hydrocarbon chain features

Fig. 4 shows wide angle data in the context of an entire CCD image with the low angle data rising vertically near the left. The length of the (11) wide angle Bragg rods in the q_z direction is consistent with the hydrocarbon chains in both monolayers of the bilayer being tilted in the same direction as was also observed for DPPC by Sun et al. (1994). Fig. 5 shows three qualitatively different wide angle patterns that occur sequentially as DMPC is dehydrated, starting with the $L_{\beta I}$ phase at full hydration and ending with the $L_{\beta F}$ phase at the lowest hydration level. Fig. 6 shows that the tilt angle θ_t as a function of D changed very little as D first decreased from its fully hydrated value. The average θ_t for the three samples with largest D in Fig. 6 is 32.3°. For the four samples with open circles with $54.4 < D < 55.4$, the average θ_t decreased to 31.3°. For smaller D, there is a transition to the $L_{\beta L}$ phase and then to the $L_{\beta F}$ phase in which θ_t decreased rapidly with decreasing D. The result in Fig. 6 implies that the DMPC gel phase bilayer structure is unlikely to change appreciably when D is greater than 56.5 Å.

From the wide angle data in the $L_{\beta I}$ phase in Fig. 6, the orthorhombic chain packing spacings were $d_{20} = 4.25$ Å

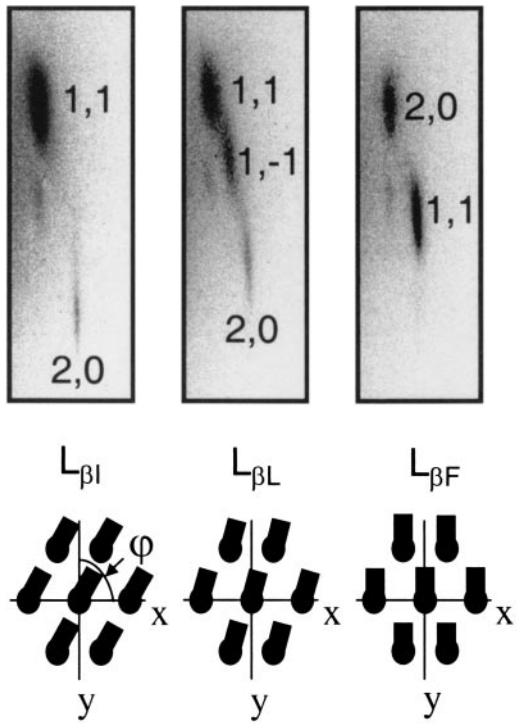

FIGURE 5 Wide angle x-ray diffraction data as in Fig. 4 showing the fully hydrated $L_{\beta I}$ gel phase, which converts to the $L_{\beta L}$ phase upon partial dehydration and then to the $L_{\beta F}$ phase upon further dehydration. The direction of chain tilting (ϕ) is shown schematically below the data.

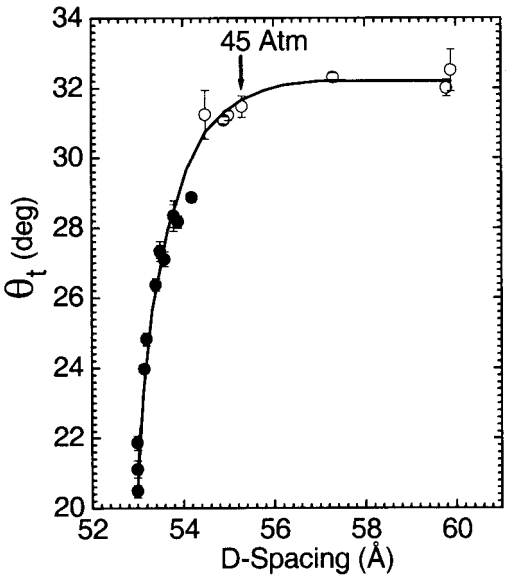

FIGURE 6 Hydrocarbon chain tilt angle θ_t as a function of D spacing of DMPC samples oriented on mica. Open circles denote the $L_{\beta I}$ phase and closed circles the $L_{\beta F}$ phase. Arrow shows the D spacing of a DMPC capillary sample under 45 ± 5 atm osmotic pressure.

and $d_{11} = 4.09$ Å with no perceptible change with varying D in the $L_{\beta I}$ phase. These spacings yield an electron density in the methylene region $\rho_2 = 0.317 \pm .0015\ e/\text{Å}^3$. This is very close to the value obtained in much the same way for gel phase DPPC at 19°C (Tristram-Nagle et al., 1993).

The area/lipid is calculated using Eq. 6 with the result $A = 47.0\ \text{Å}^2$ (column I in Table 1) for fully hydrated DMPC and $A = 46.5\ \text{Å}^2$ (column IV in Table 1) when $54.4 < D < 55.4$ Å. As indicated in Fig. 6, these smaller D spacings can be obtained by applying an osmotic pressure $p = 45$ atm to MLV samples (Nagle and Katsaras, 1999). This decrease, $\Delta A = 0.5\ \text{Å}^2$, upon applying osmotic pressure yields a result for the area compressibility modulus $K_A = 500$ dyn/cm using the defining equation (Rand and Parsegian, 1989; Nagle and Tristram-Nagle, 2000)

$$K_A = 2n_w V_w P/\Delta A \qquad (12)$$

in which n_w is the number of waters/lipid when the osmotic stress P is applied. Also, the total volume of water in the unit cell is $2n_w V_w = DA - 2V_L$, which also gives the results shown in Table 1 for the number of waters/lipid n_w.

Structure along bilayer normal

Some low angle data are shown in Figs. 2 to 4. Our global analysis obtains the phases (which are not assumed) and the unknown scaling factors K_m (see Wide Angle Data section) for each sample. Fig. 7 shows absolute scaled form factors and a continuous Fourier transform produced by a fit whose constraints will be described below. The phases of the first five orders are clearly $(- - + - -)$ typical of gel phases (Torbet and Wilkins, 1976; McIntosh and Simon, 1986b). The phase remains negative for $h = 6$ and $h = 7$. The small $h = 8$ orders have a positive phase for most values of q_z. The phases for $h = 9$ and $h = 10$ are negative. The reasonableness of these phases is apparent when they are

TABLE 1 Structural results*†‡

Quantities*	I‡	II‡	III	IV§
D	59.9¶	59.9¶	59.9¶	55.6¶
θ_t	32.3¶	32.3¶	32.3¶	31.3¶
ρ_2	0.317¶	0.314	0.325	0.317¶
A	47.0	47.5	45.9	46.5
V_H	331	319¶	357	337
$2D_C$	30.2	30.4	29.8	30.3
D_{HH}	40.1	40.1	40.3	40.6
D_{H1}	5.0	4.9	5.2	5.2
D'_B	48.2	48.4	47.8	48.3
D'_W	11.7	11.5	12.1	7.3
n_W	12.3	12.8	11.2	8.4
r	2.06	2.16	1.89	1.94
χ^2_r	1.01	1.11	0.95	1.70

*Å based units are used.
†$R = 2.0$ was constrained.
‡Columns I and II show range of favored results for full hydration (range A).
§Column IV used four samples with lower D spacings (range B).
¶Value was constrained.

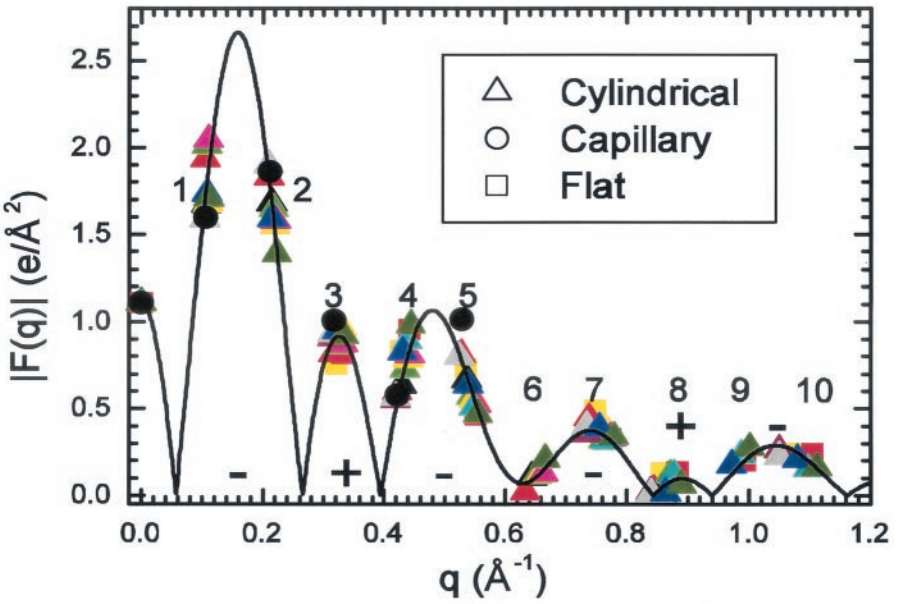

FIGURE 7 Symbols show absolute form factors for 13 samples with $56.4 < D < 60.0$ Å (range A), and the solid line shows the continuous Fourier transform obtained as described for column I of Table 1. The shape of the symbol indicates the type of sample and the different colors distinguish different samples of the same type. The regions of the different orders h are indicated by the numbers 1 to 10, and the signs of the form factors are indicated by ± for each lobe of the transform. Some samples have missing orders as explained in Materials and Methods.

used to calculate standard Fourier reconstructions (Eq. 11) of the electron density as shown in Fig. 8. The only phase that could be changed and still obtain reasonable Fourier profiles in Fig. 8 is the weak $h = 8$ order, but global fitting using several different constraint combinations and different combinations of data sets favors the phases shown in Fig. 7.

The model results in Figs. 7 and 8 were obtained with constraints for the values of θ_t and ρ_2 obtained in the last subsection. Constrained values and results of the fit are shown in column I of Table 1. Also, the ratio $R = S_{H2}/S_{H1}$ of sizes of the two headgroup peaks was set so that the inner headgroup ($i = 1$) would emulate the carbonyls, and the outer headgroup ($i = 2$) would emulate the phosphatidylcholine. These two groups have by far the greatest electron density in excess of the electron density of water or hydrocarbons, and they should therefore be related to the two Gaussians in the headgroup region. The value of $R = 2$ was obtained using the volumes of these component groups obtained from simulations (Armen et al., 1998). It may also be noted that the phosphate group has much more excess electron density than the choline group, so the outer Gaussian essentially emulates the phosphate. When this R constraint was released, the value of R migrates to 1.1, but the reduced χ^2 of the fit is not improved much ($\chi^2_r = 0.94$) and none of our conclusions is significantly altered. In particular, the electron density profile remains similar, which indicates that the 2G model is over parametrized unless the physical R constraint is used.

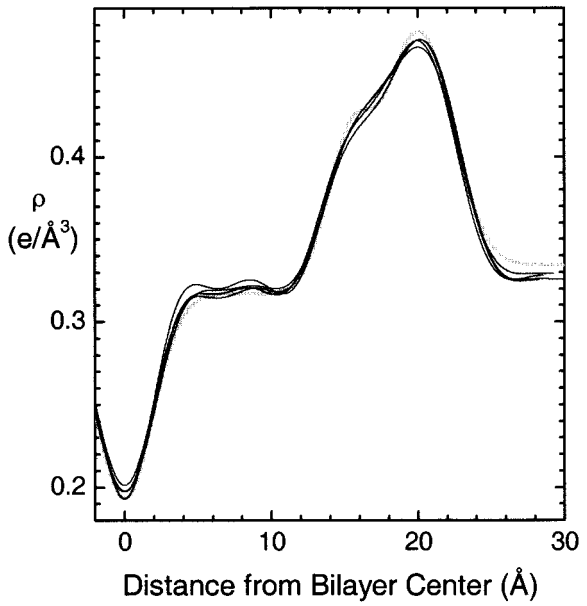

FIGURE 8 Electron density profile obtained from the fit in Fig. 7 (*broad gray curve*) and by Fourier reconstruction (*narrow black curves*) for several D spacings in range A with 10 measured orders of diffraction. The Fourier phases are those in Fig. 7. By using the scaling factors K_m obtained from the model, the Fourier profiles are placed on an absolute scale.

The fits of the model to the data with D spacing in range A shown in Fig. 7 and to the Fouriers (Eq. 11) in Fig. 8 appear satisfactory, but both improve when the wide angle constraint on ρ_2 is removed. The results of this fit are listed in column III of Table 1, which shows that the value of χ^2_r decreases. Also, ρ_2 increases, and this makes the model electron density profile agree even better with the Fouriers in the methylene plateau region $5 < z < 12$ Å than in Fig. 8. Another fitting result, shown in column II of Table 1, is motivated by a previous result for DPPC, which constrains the headgroup volume to $V_H = 319$ Å^3 (Sun et al., 1994). This fit has a higher χ^2_r, and it matches more poorly with the Fouriers in the methylene plateau region. A fit to four

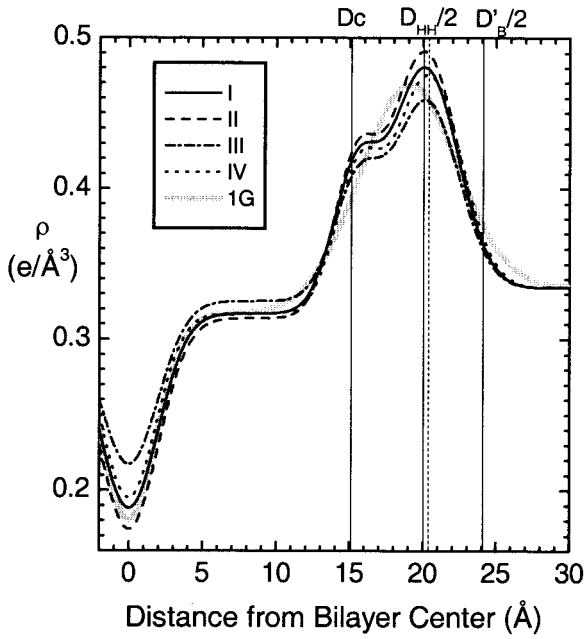

FIGURE 9 Comparison of absolute electron density profiles for the fits in columns I to IV in Table 1. Solid vertical lines show various bilayer thicknesses for column I. The dotted vertical line shows a larger $D_{HH}/2$ for the fit in column IV for partially dehydrated samples (range B). The electron density for a 1*G* model fit to fully hydrated data in range A is shown as a broad gray curve.

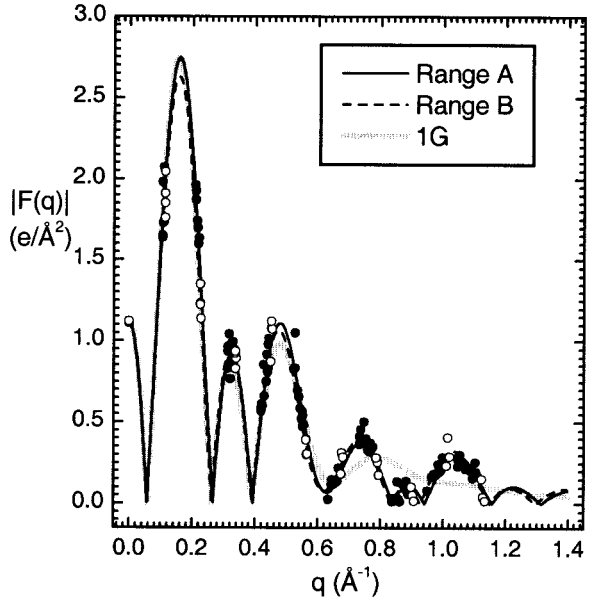

FIGURE 10 Continuous transform of the 1*G* model is shown by a broad gray curve. Continuous transform from Fig. 7 of fully hydrated model I in Table 1 is shown by a solid curve fit to the data points in range A shown by solid circles. Continuous transform of model IV in Table 1 is shown by a dashed curve fit to the partially dehydrated data in range B shown by open circles.

partially dehydrated samples with $55.3 \leq D \leq 55.8$ Å (range B) is reported in column IV in Table 1; this range of D is close to the range for the partially dehydrated wide-angle data in Fig. 6. A comparison of the electron density profiles obtained from the four fits in Table 1 is shown in Fig. 9. The full widths at half maximum are ~4.7 Å for the methyl trough, 5.1 Å for the outer phosphate Gaussian, and 3.9 Å for the inner carbonyl Gaussian with variations of order 0.1 Å among the different fits.

A fit was also performed that used only one Gaussian in the headgroup region along with the other constraints in column I of Table 1. Forcing one symmetric headgroup Gaussian to represent an obviously asymmetric headgroup gives a poor fit to the higher orders as shown in Fig. 10 with a $\chi_r^2 = 3.56$. It also shifts the location of the maximum in the headgroup electron density to smaller values by 1.0 Å, as shown in Fig. 9.

In addition to the quantities defined previously, Table 1 includes the steric bilayer thickness $D_{B'}$, which is estimated by adding 9 Å for each headgroup (Nagle and Tristram-Nagle, 2000) to the hydrocarbon thickness $2D_C$. As shown in Fig. 9, this definition of D_B' corresponds to the position at which the headgroup electron density has decayed to within 10% of the electron density of bulk water. The steric water spacing is obtained from $D_W' = D - D_B'$. We emphasize that this thickness is not the Luzzati thickness D_B that is often reported and that does not correspond to any physical thickness (Nagle and Tristram-Nagle, 2000). This difference in definitions accounts for much of the difference between the thickness of $D_B = 42.5$ Å reported by Janiak et al. (1976) and our $D_{B'}$ values in Table 1. From column I we calculate $D_B = 44.2$ Å, and this smaller remaining difference with Janiak et al. (1976) is due to their use of the gravimetric x-ray method, which generally yields larger values of A and θ_t because it overestimates the amount of water between the bilayers (Nagle and Tristram-Nagle, 2000). Table 1 also includes a measure of the distance between the phosphate group and the hydrocarbon region, namely, $D_{H1} = (D_{HH}/2) - D_C$, in which $D_{HH}/2$ is the position of the maximum in the electron density profile. Another measure not shown in Table 1 uses the position of the Gaussian representing the phosphate group instead of D_{HH}; this is slightly larger than D_{H1} by 0.1 − 0.2 Å.

DISCUSSION

There is more structural information available for gel phases than for fluid L_α phases, not only because there are more orders of low angle lamellar reflections but because the ordered chain packing gives wide angle diffraction from which the chain tilt θ_t and the lateral chain packing (methylene electron density ρ_2) are obtained. The new values obtained for fully hydrated DMPC gel phase agree very well with the extrapolation of results obtained from a study of phosphatidylcholines with chain lengths greater than 14

(Sun et al., 1996). The chain length trend from that study showed that decreasing chain length decreases θ_t and ρ_2, and decreasing temperature increases θ_t and ρ_2. Taking these trends into account quantitatively predicts the results obtained in this paper (see Table 1) for θ_t to within 0.2° and for ρ_2 to within $0.003e/Å^3$. We might also note that we chose to study DMPC at $T = 10°C$ because it is safely below the pretransition temperature of 13°C to 14°C into the ripple phase (Nagle and Wilkinson, 1978), which has an unmistakably different diffraction pattern (Katsaras et al., 2000).

Unlike our previous studies of DPPC (Wiener et al., 1989; Tristram-Nagle et al., 1993; Sun et al., 1994), this paper reports the effects of dehydration on the chain packing of DMPC. We have taken data in two hydration ranges. Most of our data are in the range $D \geq 56.5$ Å, which we call range A. The wide angle data in Fig. 6 suggest that there is little change in bilayer structure in range A, and this conclusion is supported by Fourier reconstructions in Fig. 8, so all the data in range A are appropriate for global fitting to obtain structure at full hydration for which $D = 59.9$ Å. We also have data in a narrow range $55.3 \leq D \leq 55.8$ Å, which we call range B, which corresponds to an osmotic pressure of 45 atm or a relative humidity of 96.7%. Fig. 6 suggests little variation in θ_t within this narrow range. Our subsequent global analysis suggests that the structure in range B is different than in range A. This conclusion is confirmed by comparing the structural results in columns I and IV, which show that D_{HH} and D_C increase with this small degree of dehydration. Comparison of A for columns I and IV in Table 1 for these two ranges yields the area compressibility $K_A = 500 \pm 100$ dyn/cm. If one compares A in column II with column I in Table 1, one might suppose that the uncertainty in K_A is much larger because of the large uncertainty in ΔA, which is required to calculate K_A using Eq. 12. However, the uncertainty in A between columns I and II includes the uncertainty in ρ_2; because ρ_2 does not vary experimentally with this mild dehydration, the uncertainty in ΔA only includes the uncertainty in θ_t as well as the uncertainty in n_w, which is also used to calculate K_A using Eq. 12.

Our value of K_A for gel phase DMPC may be compared with a value of 855 dyn/cm (Evans and Needham, 1987) for which the accuracy was limited by low temperature and difficulties using the aspiration pipette method for gel phases. A much more accurate value of $K_A = 234 \pm 23$ dyn/cm was obtained for the fluid L_α phase of DMPC (Rawicz et al., 2000). This is smaller than our gel phase result as one would expect. However, one might have expected the gel phase to be more than a factor of two stiffer than the fluid phase, and this is likely to be true for bilayers composed of phosphatidylethanolamines that have no chain tilt because lateral compression would require forcing hydrocarbon chains closer together against their strong repulsive cores. Tilted chains offer a different degree of freedom to reduce their area A, namely, reduction of chain tilt while maintaining the same distance between parallel chains. Of course, the headgroups must still come closer together and this is effected by the osmotic dehydration. Therefore, gel phase phosphatidylcholines remain moderately soft under lateral compression. This explanation conforms well to the model used to explain the very small thermal area expansivity (Sun et al., 1996) and the chain length dependence of A (Tristram-Nagle et al., 1993).

It may be of some interest to speculate on how this small value of K_A relates to the bending modulus K_c. It is generally accepted that the bending modulus K_c is related to the area modulus K_A by a formula of the form $K_c = K_A(2D_C)^2/N$. In a recent advance in the theory that involved consideration of a polymer brush model, Rawicz et al. (2000) derived $N = 24$, and their data showed that this works well for many fluid phase lipids that do not have a high degree of unsaturation. Using $N = 24$ and our values of K_A and D_C yields $K_c = 1.9 \times 10^{-12}$ erg. However, we suggest that the observation of a fairly sharp $h = 10$ diffraction peak (Fig. 2) requires a larger value of K_c for gel phase DMPC. Our suggestion is based on using this putative K_c value to calculate the Caillé fluctuation parameter for the hth order $\eta_h = h^2\pi k_B T/[2D^2(BK_c)^{1/2}]$ (Nagle and Tristram-Nagle, 2000); we estimate the interaction bulk modulus $B = 10^{14}$ erg/cm^4 from Petrache et al. (1998b) when the separation between bilayers is taken to be the same as for the fully hydrated gel phase in Table 1. This gives $\eta_{10} = 1.3$ and such a large value of η would give a broader $h = 10$ peak (Lyatskaya et al., 2001) than we observe in Fig. 2 *B*. Because the polymer brush analogy would not be expected to apply to gel phase lipids, it may be better to revert to simple elasticity theory that predicts $N = 12$ under the assumptions that 1) the monolayers in the bilayer do not slip relative to each other and 2) the lateral force required to compress the bilayer is the same at all distances z from the center of the bilayer. Assumption 1 is supported by our result for the length of the wide angle arcs that implies registry of the hydrocarbon chains between monolayers. However, if the headgroups are much less compressible than the chains, then the breakdown of assumption 2 yields $N = 4$ and $K_c = 11 \times 10^{-12}$ erg. Therefore, it seems possible to reconcile our small value of K_A with the lack of significant broadening of the tenth order diffraction peak. This suggestion is consistent with the view that bending fluctuations are largely suppressed in gel phases (McIntosh and Simon, 1993).

The sequence of structural phases we observe in Fig. 5 is the same as those observed for temperatures above 15°C by Smith et al. (1990) in their pioneering study that mapped out a phase diagram for the various gel subphases. However, they did not report data at lower temperatures, and they were unable to achieve fully hydrated D spacings. Their extrapolated phase diagram implied that $L_{\beta F}$ is the fully hydrated DMPC gel phase below $T = 13°C$. In contrast, our data show that $L_{\beta I}$ is the fully hydrated DMPC gel phase at

10°C; this is also the stable gel phase for fully hydrated DPPC. Smith et al. (1990) also reported $\theta_t = 30.0°$ at $T = 23.5$°C. Our $\theta_t = 31.3°$ for our comparably dehydrated D spacings in range B at 10°C is in excellent agreement with their result when adjustment is made for the temperature dependence of the tilt angle $d\theta_t/dT = -0.1°$ obtained by Sun et al. (1996).

Our most significant result for θ_t shown in Fig. 6 and for ρ_2 is that they do not change appreciably with dehydration until D is smaller than 56.5 Å. Therefore, A and the hydrocarbon core do not change from full hydration. Also, because the steric thickness of the bilayer is only approximately $D_{B'} = 48$ Å (Table 1), the headgroups are still well solvated even down to $D = 55.6$ Å in range B, so they are likely to have the same conformations. Our result that the phosphate/hydrocarbon distance D_{H1} changes very little between columns I and IV of Table 1 is consistent with having even less variation in headgroup conformation within each range of D. Therefore, changes in bilayer structure for $D >$ 56.5 Å would seem to be negligible because neither the hydrocarbon region nor the headgroup region appears to be changing. Accordingly, we have developed a global analysis that uses data throughout range A, close to and including full hydration. This provides much more low angle data than our previous low angle analysis for gel phase DPPC (Wiener et al., 1989).

Let us make one more comparison of results from range B and range A. Fig. 9 also shows a small, but definite, shift in the electron density profile. From five orders of diffraction, McIntosh and Simon (1986b) concluded that changes in D_{HH} were less than 1 Å for changes in osmotic pressure from 0 to 50 atm, which is consistent with our difference of 0.5 Å based on 10 orders of diffraction. In agreement with McIntosh and Simon, these differences correspond to a rather small change in the continuous transforms as shown in Fig. 10. These differences are much smaller than the differences in the continuous transforms of DPPC obtained by Torbet and Wilkins (1976). This is consistent with their oriented samples being more dried out with shrinkages in D at least 5.2 Å compared with our average shrinkage of 4.3 Å in range B. Fig. 6 shows that DMPC tilt angle θ_t begins to change quite rapidly with D when the shrinkage exceeds 5 Å. Fluid phase structure begins to change rapidly when n_W becomes smaller than 11 to 13 (Hristova and White, 1998), which is the number of waters required to complete the inner hydration shell (Perera et al., 1997; Mashl et al., 2001). Table 1 suggests that gel phase structure begins to change significantly when $n_w < 9$; this limiting n_w for effective fully hydrated structure should be smaller than for the fluid phase limit because less water is required between the headgroups because A is smaller.

Although the results of the fits shown in Figs. 7 and 8 appear to be reasonable, there is a small conflict between the wide angle result for ρ_2 and the low angle data. This is indicated by the lower χ_r^2 when the fit is not constrained by the wide angle value $\rho_2 = 0.317e/Å^3$ (compare column I and column III in Table 1). It is also indicated by better agreement of the electron density of model III and the Fouriers in the methylene region; Fig. 8 shows that the methylene plateau value of model I is slightly below that of the Fourier levels. A similar conflict was noted for DPPC by Wiener et al. (1989), but then there were so few low angle data compared with the number of model parameters that it was concluded that the low angle data were incapable of providing independent estimates of ρ_2. A more refined analysis of DPPC (Sun et al., 1994) that incorporated two satellite peaks (one is shown in Fig. 4) revealed that the d_{11} spacing is not necessarily obtained from the location of greatest intensity in the (11) peak. That analysis obtained the same value of $\theta_t = 32°$ for DPPC that Tristram-Nagle et al. (1993) obtained by the more straightforward analysis also used in this article. However, again for DPPC, the method of Sun et al. (1994) yielded a smaller value of ρ_2 and a correspondingly larger $A = 47.9$ Å^2, compared with $A = 47.2$ Å^2 that was obtained by the conventional method (Tristram-Nagle et al., 1993) used in the Results section of this article. The smaller ρ_2 then produced a smaller $V_H = 319$ Å^3 (Sun et al., 1994) for DPPC. Because the areas and tilt angles are so similar in DPPC and DMPC, and because the same phosphatidylcholine headgroup is fully hydrated in both systems, it is reasonable that the headgroup volume V_H is the same, and this is the constraint that is used in the fit reported in column II of Table 1. Unfortunately, this constraint increases the χ_r^2 of the fit compared with columns I and III, so it widens the conflict between wide angle and low angle results. Fig. 9 emphasizes the effects that the wide-angle choices have on the electron density profiles.

One possible resolution of the conflict is that it may not be the data but the functional form of the model that is at fault. Although Gaussians are undoubtedly the best simple approximation for the distribution of component groups in condensed matter systems such as bilayers, they would only be exact if the potential of mean force happens to be perfectly harmonic over the ranges of fluctuations represented by the widths of the fitted Gaussians. Indeed, simulations of fluid phase bilayers (Feller et al., 1997; Armen et al., 1998) show that spatial distributions of many component groups are close to, although not quite, Gaussians, and the largest deviation was the terminal methyl distribution. A recent simulation of the gel phase of DPPC shows that the terminal methyls are quite well localized with the *sn*-1 methyls centered at $z = \pm 0.6$ Å and the *sn*-2 methyls centered at $z = \pm 2.7$ Å (Venable et al., 2000). Perhaps this kind of fine structure will be useful in future data analysis, but the smoothed electron density profile presented in their Fig. 4 suggests that the Gaussian trough used in this paper is a good first approximation.

We will not resolve this conflict in this paper. Instead, we conclude that the range of values represented by columns I to III in Table 1 are all possible, depending upon how one

weights the low angle data versus the wide angle data and which wide angle result one decides is most plausible. We prefer the range between column I and II because we think the wide angle ρ_2 data should not be ignored. Before this study, we preferred the wide angle results from Sun et al. (1994), which gives column II, but the larger χ_r^2 in the global low angle fits has reduced our confidence, so that we now give equal weight to the straightforward result for ρ_2 represented by column I.

Although the heights of the headgroup peaks and the depth of the methyl trough in Fig. 9 decrease for models with smaller $\rho_w - \rho_2$, some important results are robustly independent of these uncertainties in ρ_2. For the fully hydrated models I to III, there is very little difference in the distance between the headgroup peaks in the electron density profiles as seen by comparing D_{HH} in Table 1. There are also only minor differences in hydrocarbon thickness $2D_C$ (these are caused by small differences in r via Eq. 8). This means that the value of ρ_2 makes little difference in the quantity D_{H1} that represents the distance between the phosphates and the hydrocarbon chain regions. The method of obtaining fluid phase area structure using gel phase structure as a stepping-stone assumes that D_{H1} is the same in both phases. This assumption is supported by the good agreement of the results shown in Table 1 with $D_{H1} = 5.2$ Å from fluid phase simulations (Feller et al., 1997; see also figure 2 in Nagle and Tristram-Nagle, 2000). It is also encouraging that there is agreement with the value $D_{H1} = 5.0$ Å for gel phase DPPC that can be obtained from Table 3 of Wiener et al. (1989). However, it should be emphasized that the one Gaussian fit in Fig. 9 yields a much smaller value of $D_{H1} = 4.2$ Å and an even smaller $D_{H1} = 4.1$ Å when only four orders of diffraction are used in the fit. This is easily understood from Fig. 9 because the single Gaussian attempts to compromise between the larger Gaussian that represents the phosphate and the smaller Gaussian that represents the carbonyls. This artifact must be taken into account when analyzing fluid phase data, which generally have fewer orders due to suppression of higher orders by fluctuations (Zhang et al., 1994, 1996). Because fitting to a two Gaussian model is then underdetermined, the one Gaussian model for both the gel and the fluid phase has been used by Nagle et al. (1996). Now that we have more confidence in the electron density profile in the headgroup region for the gel phase, another possibility emerges that uses the gel phase electron density profile in the headgroup region to constrain the fitting of fluid phase data. Constraints would include $R = 2$ and the distance between the two headgroup peaks, while retaining the mean position of the headgroup and its width as fitting parameters. It is therefore anticipated that this DMPC gel phase structure will be useful in obtaining better structures of many fluid phase bilayers with PC headgroups.

The authors thank John Katsaras of the Chalk River Laboratories (National Research Council of Canada) for the use of the x-ray chamber that provides full hydration of oriented samples from the vapor. We thank Tomasz Kowalewski of the Chemistry Department at Carnegie Mellon University for use of his AFM facility and his advice. We thank Rich Pastor and Rick Venable for interesting discussions and for sharing detailed probability distribution functions that were calculated, but not published, in Venable et al. (2000). We acknowledge use of the CHESS facility (National Science Foundation Grant DMR-9311772) and thank all the CHESS staff, particularly Ernie Fontes for much help with the D1 station. We thank CHESS director Sol Gruner and his associates Adam Finnefrock and Mark Tate for assistance and discussion regarding use of the CCD. This work was supported by the National Institutes of Health Grant GM44976-11 and the Petroleum Research Foundation.

REFERENCES

Armen, R. S., O. D. Uitto, and S. E. Feller. 1998. Phospholipid component volumes: determination and application to bilayer structure calculations. *Biophys. J.* 75:734–744.

Barna, S. L., M. W. Tate, S. M. Gruner, and E. F. Eikenberry. 1999. Calibration procedures for charge-coupled device x-ray detectors. *Rev. Sci. Instr.* 70:2927–2934.

Blanton, T. N., T. C. Huang, H. Toraya, C. R. Hubbard, S. B. Robie, D. Louer, H. E. Gobel, G. Will, R. Gilles, and T. Raftery. 1995. JCPDS-international centre for diffraction data round robin study of silver behenate. *Powder Diffraction* 10:91–95.

Bouwstra, J. A., M. A. Salomons-de Vries, J. A. van der Spek, and W. Bras. 1992. Structure of human stratum corneum as a function of temperature and hydration: a wide angle x-ray diffraction study. *Int. J. Pharmacol.* 84:205–216.

Evans, E., and D. Needham. 1987. Physical properties of surfactant bilayer membranes: thermal transitions, elasticity, rigidity, cohesion, and colloidal interactions. *J. Phys. Chem.* 91:4219–4228.

Feller, S. E., R. M. Venable, and R. W. Pastor. 1997. Computer simulation of a DPPC phospholipid bilayer: structural change as a function of molecular surface area. *Langmuir.* 13:6555–6561.

Hentschel, M. P., and F. Rusticelli. 1991. Structure of the ripple phase $P_{\beta'}$ in hydrated phosphatidylcholine multimembranes. *Phys. Rev. Lett.* 66: 903–906.

Hristova, K., and S. H. White. 1998. Determination of the hydrocarbon core structure of fluid dioleoylphosphocholine (DOPC) bilayers by x-ray diffraction using specific bromination of the double-bonds: effect of hydration. *Biophys. J.* 74:2419–2433.

Huster, D., A. J. Jin, K. Arnold, and K. Gawrisch. 1997. Water permeability of polyunsaturated lipid membranes measured by ^{17}O NMR. *Biophys. J.* 73:855–864.

Janiak, M. J., D. M. Small, and G. G. Shipley. 1976. Nature of the thermal pretransition of synthetic phospholipids: dimyristoyl- and dipalmitoyllecithin. *Biochemistry.* 15:4574–4580.

Katsaras, J. 1998. Adsorbed to a rigid substrate, dimyristoylphosphatidylcholine multibilayers attain full hydration in all mesophases. *Biophys. J.* 75:2157–2162.

Katsaras, J., and M. J. Watson. 2000. Sample cell capable of 100% relative humidity suitable for x-ray diffraction of aligned lipid multibilayers. *Rev. Sci. Instrum.* 71:1737–1739.

Katsaras, J., S. Tristram-Nagle, Y. Liu, R. L. Headrick, E. Fontes, P. C. Mason, and J. F. Nagle. 2000. Clarification of the ripple phase of lecithin bilayers using fully hydrated aligned samples. *Phys. Rev. E.* 61: 5668–5677.

Katsaras, J., D. S.-C. Yang, and R. M. Epand. 1992. Fatty-acid chain tilt angles and direction in DPPC bilayers. *Biophys. J.* 63:1170–1175.

Levine, Y. K. 1973. X-ray diffraction studies of membranes. *Prog. Surf. Sci.* 3:279–352.

Lewis, B. A., and D. M. Engelman. 1983. Lipid bilayer thickness varies linearly with acyl chain length in fluid phosphatidylcholine vesicles. *J. Mol. Biol.* 166:211–217.

Lundbaek, J. A., and O. S. Andersen. 1999. Spring constants for channel-induced lipid bilayer deformations: estimates using gramicidin channels. *Biophys. J.* 76:889–895.

Lyatskaya, Y., Y. Liu, S. Tristram-Nagle, J. Katsaras, and J. F. Nagle. 2001. Method for obtaining structure and interactions from oriented lipid bilayers. *Phys. Rev. E.* 63:0119071–0119079.

Mashl, R. J., H. L. Scott, S. Subramaniam, and E. Jakobsson. 2001. Molecular simulation of dioleoylphosphatidylcholine lipid bilayers at differing levels of hydration. *Biophys. J.* 81:3005–3015.

McIntosh, T. J. 2000. Short-range interactions between lipid bilayers measured by x-ray diffraction. *Curr. Opin. Struct. Biol.* 10:481–485.

McIntosh, T. J., and S. A. Simon. 1986a. Area per molecule and distribution of water in fully hydrated DLPE bilayers. *Biochemistry*. 25: 4948–4952 and 8474.

McIntosh, T. J., and S. A. Simon. 1986b. Hydration force and bilayer deformation: a reevaluation. *Biochemistry.* 25:4058–4066.

McIntosh, T. J., and S. A. Simon. 1993. Contributions of hydration and steric entropic pressure to the interactions between phosphatidylcholine bilayers: experiments with the subgel phase. *Biochemistry*. 32: 8374–8384.

Nagle, J. F., and J. Katsaras. 1999. Absence of a vestigial vapor pressure paradox. *Phys. Rev. E.* 59:7018–7024.

Nagle, J. F., and S. Tristram-Nagle. 2000. Structure of lipid bilayers. *Biochim. Biophys. Acta.* 1469:159–195.

Nagle, J. F., and M. C. Wiener. 1989. Relations for lipids bilayers: connection of electron density profiles to their structural quantities. *Biophys. J.* 64:1476–1481.

Nagle, J. F., and D. A. Wilkinson. 1978. Lecithin bilayers: density measurements and molecular interactions. *Biophys. J.* 23:159–175.

Nagle, J. F., R. Zhang, S. Tristram-Nagle, W-. S. Sun, H. I. Petrache, and R. M. Suter. 1996. X-ray structure determination of L_α-phase DPPC bilayers. *Biophys. J.* 70:1419–1431.

Olbrich, K., W. Rawicz, D. Needham, and E. A. Evans. 2000. Water permeability and mechanical strength of polyunsaturated lipid bilayers. *Biophys. J.* 79:321–327.

Paula, S., A. G. Volkov, A. N. V. Hoek, T. H. Haines, and D. W. Deamer. 1996. Permeation of protons, potassium ions, and small polar molecules through phospholipid bilayers as a function of membrane thickness. *Biophys. J.* 70:339–348.

Perera, L., U. Essman, and M. L. Berkowitz. 1997. The role of water in the hydration force: molecular dynamics simulations. *Progr. Colloid Polymer Sci.* 103:107–115.

Petrache, H. I., N. Gouliaev, S. Tristram-Nagle, R. Zhang, R. M. Suter, and J. F. Nagle. 1998b. Interbilayer interactions from high-resolution x-ray scattering. *Phys. Rev. E.* 57:7014–7024.

Petrache, H. I., S. Tristram-Nagle, and J. F. Nagle. 1998a. Fluid phase structure of EPC and DMPC bilayers. *Chem. Phys. Lipids.* 95:83–94.

Pilgram, G. S. K., A. M. Engelsma-van Pelt, J. A. Bouwstra, and H. K. Koerten. 1999. Electron diffraction provides new information on human stratum corneum lipid organization studied in relation to depth and temperature. *J. Invest. Dermatol.* 113:403–409.

Rand, R. P., and V. A. Parsegian. 1989. Hydration forces between phospholipid bilayers. *Biochim. Biophys. Acta.* 988:351–376.

Rawicz, W., K. C. Olbrich, T. McIntosh, D. Needham, and E. Evans. 2000. Effect of chain length and unsaturation on elasticity of lipid bilayers. *Biophys. J.* 79:328–339.

Ruocco, M. J., and G. G. Shipley. 1982. Characterization of the subtransition of DPPC bilayers. *Biochim. Biophys. Acta.* 691:309–320.

Smith, G. S., E. B. Sirota, C. R. Safinya, and N. A. Clark. 1988. Structure of the L_β-phase in DMPC. *Phys. Rev. Lett.* 60:813–816.

Smith, G. S., E. B. Sirota, C. R. Safinya, R. J. Plano, and N. A. Clark. 1990. X-ray structural studies of freely suspended ordered hydrated DMPC multimembrane films. *J. Chem. Phys.* 92:4519–4529.

Stark, G. 1991. The effect of ionizing radiation on lipid membranes. *Biochim. Biophys. Acta.* 1071:103–122.

Sun, W.-J., R. M. Suter, M. A. Knewtson, C. R. Worthington, S. Tristram-Nagle, R. Zhang, and J. F. Nagle. 1994. Order and disorder in fully hydrated unoriented bilayers of gel phase dipalmitoylphosphatidylcholine. *Phys. Rev. E.* 49:4665–4676.

Sun, W.-J., S. Tristram-Nagle, R. M. Suter, and J. F. Nagle. 1996. Structure of gel phase saturated lecithin bilayers: temperature and chain length dependence. *Biophys. J.* 71:885–891.

Tate, M. W., E. F. Eikenberry, S. O. Barna, S. E. Wall, J. L. Lowrance, and S. M. Gruner. 1995. A large-format high-resolution area x-ray detector based on a fiber-optically bonded charge-coupled device (CCD). *J. Appl. Crystogr.* 28:196–205.

Tieleman, D. P., S. J. Marrink, and H. J. C. Berendsen. 1997. A computer perspective of membranes: molecular dynamics studies of lipid bilayer systems. *Biochim. Biophys. Acta.* 1331:235–270.

Tobias, D. J., K. Tu, and M. L. Klein. 1997. Atomic-scale molecular dynamics simulations of lipid membranes. *Curr. Opin. Colloid Interface Sci.* 2:15–26.

Torbet, J., and M. H. F. Wilkins. 1976. X-ray diffraction studies of lecithin bilayers. *J. Theor. Biol.* 62:447–458.

Tristram-Nagle, S., H. I. Petrache, and J. F. Nagle. 1998. Structure and interactions of fully hydrated dioleoylphosphatidylcholine bilayers. *Biophys. J.* 75:917–925.

Tristram-Nagle, S., R. Zhang, R. M. Suter, C. R. Worthington, W-J. Sun, and J. F. Nagle. 1993. Measurement of chain tilt angle in fully hydrated bilayers of gel phase lecithin. *Biophys. J.* 64:1097–1109.

Veld, G. I., A. J. M. Driessen, J. A. F. Op Den Kamp, and W. N. Konings. 1991. Hydrophobic membrane thickness and lipid-protein interactions of the leucine transport system of *Lactococcus lactis*. *Biochim. Biophys. Acta.* 1065:203–212.

Venable, R. M., B. R. Brooks, and R. W. Pastor. 2000. Molecular dynamics simulations of gel ($L_{\beta I}$) phase lipid bilayers in constant pressure and constant surface area ensembles. *J. Chem. Phys.* 112:4822–4832.

Wiener, M. C., R. M. Suter, and J. F. Nagle. 1989. Structure of the fully hydrated gel phase of DPPC. *Biophys. J.* 55:315–325.

Wiener, M. C., and S. H. White. 1991. Transbilayer distribution of bromine in fluid bilayers containing a specifically brominated analogue of DOPC. *Biochemistry.* 30:6997–7008.

Worthington, C. R., G. I. King, and T. J. McIntosh. 1973. Direct structure determination of multilayered membrane-type systems which contain fluid layers. *Biophys. J.* 13:480–494.

Zhang, R., R. M. Suter, and J. F. Nagle. 1994. Theory of the structure factor of lipid bilayers. *Phys. Rev. E.* 50:5047–5060.

Zhang, R., S. Tristram-Nagle, W. Sun, R. L. Headrick, T. C. Irving, R. M. Suter, and J. F. Nagle. 1996. Small-angle x-ray scattering from lipid bilayers is well described by modified Caillé theory but not by paracrystalline theory. *Biophys. J.* 70:349–357.